Molecular geometry fluctuations and field-dependent mobility in conjugated polymers

Z. G. Yu,[1,2] D. L. Smith,[1] A. Saxena,[1] R. L. Martin,[1] and A. R. Bishop[1]
[1]*Los Alamos National Laboratory, Los Alamos, New Mexico 87545*
[2]*Department of Chemistry, Iowa State University, Ames, Iowa 50011*
(Received 22 February 2000; revised manuscript received 11 September 2000; published 1 February 2001)

Many conjugated polymers exhibit an electric field-dependent mobility of approximately the Poole-Frenkel form. We propose a model to describe transport in dense films of these materials in which thermal fluctuations in the molecular geometry modify the energy levels of localized electronic charged states in the material. Based on quantum chemistry calculations we argue that the primary restoring force for these fluctuations in molecular geometry is steric in origin, which leads to spatially correlated fluctuations in the on-site energy of the charged electronic states. The phenylene ring torsion, in PPV-like conjugated polymers, is an example of this kind of spatially correlated thermal fluctuation. Using a Master equation approach to calculate the mobility, we show that the model can quantitatively explain the experimentally observed field-dependent mobility in conjugated polymers. We examine typical paths taken by carriers and find that at low fields, the paths are three-dimensional, whereas at high fields the paths become essentially one-dimensional along the applied field. Thus, one-dimensional transport models can be valid at high fields but not at low fields. Effects of deep traps, the site energy correlation length, temperature, and asymmetric and small polaron rates are studied.

DOI: 10.1103/PhysRevB.63.085202 PACS number(s): 72.10.−d, 71.38.−k, 72.80.Le

I. INTRODUCTION

Electronic devices based on conjugated polymers have attracted much attention because of their processing and performance advantages.[1,2] Understanding the carrier transport properties in these materials is important to design and synthesize better materials and to further improve the device performance. Time-of-flight mobility measurements show that the field-dependent mobility in many conjugated polymers approximates the Poole-Frenkel form, i.e., the mobility increases approximately exponentially with $\sqrt{E}$ over an extended range of electric field E.[3–5] Theoretically, Bässler and co-workers extensively studied field-dependent mobility in these materials using Monte Carlo simulations of the Gaussian disorder model (GDM).[6] The GDM satisfactorily explains many features of mobility observed in these materials; however, as pointed out by Gartstein and Conwell,[7] a spatially correlated potential for the carriers is needed to explain the Poole-Frenkel behavior in the low-field region ($\sim 10^4$ V/cm).

Historically, Poole-Frenkel behavior was first observed in molecularly doped polymers, in which the dopants have permanent electric dipole moments.[8,9] Dunlap and co-workers recently proposed the charge-dipole model for the mobility in these molecularly doped materials.[10] The long-range spatial correlation of carrier energies, which comes about from the charge-dipole interaction, is an essential aspect of this model. The charge-dipole model has been very successful in describing the observed transport properties of molecularly doped polymers. Although the mobility in conjugated polymers and in molecularly doped materials exhibits some similarities in behavior, the mechanism leading to the Poole-Frenkel behavior in conjugated polymers cannot be due to charge-dipole interactions, as it is in molecularly doped polymers, because most conjugated polymers do not have a permanent dipole moment. Therefore, an alternative mechanism is needed to explain the field-dependent mobility in conjugated polymers. Here we propose a model, in which thermal fluctuations in the molecular geometry modify the energy levels of localized electronic charged states in the material, and study the predictions of this model for the field and carrier density dependence of the mobility. A preliminary discussion of this model has been presented in a short note.[11]

Conjugated polymers contain impurities and defects. These impurities and defects may serve as traps for carriers in these materials, which may be critical to electrical transport. We construct a one-dimensional (1D) trap model and obtain the analytical solution for this model. We also numerically study the three-dimensional (3D) system with randomly distributed deep traps.

In 1D models, analytical results for the mobility can be obtained based on Derrida's exact solution to a 1D steady state Master equation.[12] Since 3D models are too complex to have an analytical solution, there is a temptation to extend the 1D results to 3D. However, it is not clear to what extent the 1D results can be used in 3D systems. In 3D systems, the carrier can choose optimal paths to avoid high energy barriers, while in 1D systems, the carrier has no choice for its path. We systematically compare the numerical 3D results with the 1D results and study typical carrier paths in 3D systems.

The article is organized as follows. In Sec. II, we introduce our model and estimate the parameters of the model Hamiltonian. In Sec. III, we present 1D analytical solutions of the model. Section IV is devoted to 3D numerical results including asymmetric and small polaron rates. We summarize our conclusions in Sec. V.

II. MODEL

Since most conjugated polymers show a field-dependent mobility of the Poole-Frenkel form, the model and the mechanism used to describe this observed behavior should

be generic. Compared with many other conjugated polymers, the observed field-dependent mobility of poly(9,9-dioctylfluorene) (PFO) is unusual: The mobility in PFO is two orders higher than that in poly(*p*-phenylene vinylene) (PPV), and the field dependence is very weak.[13] In conjugated polymers like PPV, the orientation of the benzene rings can fluctuate around their equilibrium positions. In PFO, however, the ring-torsion freedom is suppressed by the chemical bonding between the phenylene rings. This difference suggests that fluctuations in molecular geometry can strongly affect the mobility in these materials. In conjugated polymers, the restoring force of ring orientation fluctuations may come from two origins, intermolecular or intramolecular interactions. The intermolecular restoring force becomes dominant in dense films, where molecules are closely packed.[14] Because of the short distance between molecules, small fluctuations of the adjacent molecular orientations may give rise to a large steric energy. By contrast, the intramolecular restoring force is weak. The characteristic energy measured for the torsion mode in an isolated PPV molecule is quite small.[15]

To quantitatively understand the effects of fluctuations in molecular geometry in conjugated polymers, we carried out an electronic structure calculation of the total energy (AM1)[16] of biphenyl as a function of the twist angle between two rings. For neutral biphenyl, the energy is almost constant with changing torsion angle.[11] However, when an extra electron or hole is added to this system, the total energy of the charged state strongly depends on the torsion angle. This result is expected, as conventional resonance structures suggest there should be very little π-character in the bond connecting the two benzene rings for the neutral molecule, and therefore there is nearly free rotation about the single bond. But for both positive and negative ions a coplanar orientation maximizes the π-overlap between them and allows the charge to delocalize more easily over both rings. Thus there is a strong coupling between the local electronic excitation (carrier) and the ring orientation. To estimate the steric interaction between chains, we examined a model consisting of three parallel benzene rings with a fixed separation.[11] These calculations show that the intermolecular restoring is dominant over the intramolecular one in densely packed materials.

We propose a general model to describe the mobility in dense films of conjugated polymers described by the Hamiltonian

$$H=\sum_i \varepsilon_i C_i^\dagger C_i+\frac{K}{2}\int d^3r(\nabla\phi)^2+\nu\sum_i C_i^\dagger C_i\phi(\mathbf{r}_i) + \frac{s}{2}\int d^3r\phi^2(\mathbf{r})+\sum_{i,j}\eta_{ij}(C_i^\dagger C_j+\text{H.c.}). \quad (1)$$

Here $C_i^\dagger$ is the creation operator of a carrier (polaron) on site i and ε_i is its bare energy. $\phi(\mathbf{r})$ describes the molecular geometry field (in PPV, it can be regarded as the deviation of the torsion angle of the benzene ring from its equilibrium value at $\mathbf{r}$). K is the intermolecular restoring force constant; the origin of the gradient of the molecular geometry field in this term is that the intermolecular elastic energy depends on the difference of the torsion in adjacent molecules. s is the intramolecular restoring force constant. This term is small compared with the intermolecular term. The energy minimum in the neutral system occurs in a different geometry than that in the charged system.[11] Expanding the energy of the charged system around the equilibrium geometry (energy minimum for the neutral system) gives a linear coupling between the polaron and the torsion described by the coupling constant ν. η_{ij} is the polaron hopping matrix element between sites. The effect of fluctuations in the bare site energies ε_i has been studied in the GDM.[6] Here we consider cases in which energy fluctuations are dominated by the interaction with the molecular geometry field and take the bare site energies all equal to zero.

The renormalized polaron energy is a function of position due to the local coupling between the polaron and the molecular geometry

$$\varepsilon(\mathbf{r}_i)=\nu\phi(\mathbf{r}_i). \quad (2)$$

The total free energy from the molecular geometry fluctuations is

$$\mathcal{F}_{\text{mg}}=\Omega^{-1}\sum_{\mathbf{q}}|\Phi(\mathbf{q})|^2(K\mathbf{q}^2/2+s/2), \quad (3)$$

where Ω is the volume of the system and $\Phi(\mathbf{q})$ is the Fourier transform of $\phi(\mathbf{r})$.[11] The equipartition law, $\langle\mathcal{F}_{mg}\rangle=k_BT/2$, gives the spatial correlation of polaron energies, at temperature T,

$$\langle\varepsilon(\mathbf{r}_1)\varepsilon(\mathbf{r}_2)\rangle=\nu^2\langle\phi(\mathbf{r}_1)\phi(\mathbf{r}_2)\rangle=\frac{\nu^2k_BT}{4\pi KR}e^{-\alpha R}, \quad (4)$$

where $R=|\mathbf{r}_1-\mathbf{r}_2|$, $\alpha=\sqrt{s/K}$, and k_B is Boltzmann's constant.

The parameters ν and K in the Hamiltonian can be estimated from the AM1 quantum chemistry calculations for the biphenyl molecule and the three-benzene system.[11] We find $\nu\sim0.3$–0.4 eV per radian and $K\sim0.002$–0.005 eV/Å.

III. 1D ANALYTICAL RESULTS

A. Poole-Frenkel behavior

A 1D Master equation with nearest neighbor hopping that can be used to describe the field-dependent mobility has been exactly solved by Derrida.[12] In the continuum limit, the mobility can be calculated using this solution to the Master equation.[10,17] Using the correlation function obtained for our model gives for the mobility

$$\mu=\frac{\mu_0e^{-\beta\sigma^2}}{\beta\sqrt{2\pi\sigma^2aeE}K_1(\beta\sqrt{2\pi\sigma^2aeE})}, \quad (5)$$

where $\beta=(k_BT)^{-1}$, $\sigma^2=\nu^2/(2\pi^2Ka)$, $1/a$ is the momentum cutoff, and $K_1(z)$ is the first-order modified Bessel function of the third kind. By using the asymptotic expansion for $K_1(z)$, the mobility is

$$\mu\sim e^{-\beta\sigma^2}e^{\beta\sqrt{E}\sqrt{2\pi\sigma^2ae}}. \quad (6)$$

For this 1D solution, our model and the charge-dipole model result in the same field dependence for the mobility, i.e., $\ln\mu\sim\sqrt{E}$. However, our model leads to a different temperature dependence of the mobility: $\ln\mu\sim\beta$ in our model whereas $\ln\mu\sim\beta^2$ in the charge-dipole model. The reason for the different temperature dependence is that the energetic disorder is independent of temperature in the charge-dipole model, whereas it increases with increasing temperature in our model.

B. Trap effects

We consider a 1D model to study the effect of traps on the mobility. Two kinds of sites are considered, ''regular sites'' and a small concentration of ''trap sites.'' Each trap site has two levels, one is deep (a) and the other is shallow (b). The shallow level at the trap site is similar to the levels at regular sites. The deep level (a) is not directly connected to other sites, instead, it connects only via the shallow level on the trap. The occupation of the deep trap sites may be substantial, but the occupation of regular sites is small. We study a nonlinear Master equation where P_i is the probability for the particle to be on site i and ω_{ij} is the hopping rate from site j to site i. For regular sites, this nonlinear equation can be linearized. If site l is a trap, the Master equation for the two levels (a and b) on the trap site read

$$\frac{dP_l^a}{dt}=\omega_{ab}(1-P_l^a)P_l^b-\omega_{ba}(1-P_l^b)P_l^a, \tag{7}$$

$$\frac{dP_l^b}{dt}=\omega_{ll-1}P_{l-1}+\omega_{ll+1}P_{l+1}-(\omega_{l+1l}+\omega_{l-1l})P_l^b + \omega_{ba}(1-P_l^b)P_l^a-\omega_{ab}(1-P_l^a)P_l^b. \tag{8}$$

The Master equation for regular sites is the same as that for the b level trap sites without the terms involving the a levels.

At steady state

$$\omega_{ab}(1-P_l^a)P_l^b=\omega_{ba}(1-P_l^b)P_l^a. \tag{9}$$

Thus the occupation probabilities for the deep level a of trap sites drops out of the Master equation; it has the same form as for the model without traps and we can use Derrida's solution. The effect of the traps enters by changing the normalization condition. That is, the sum over all site occupation probabilities, including the deep level trap sites, is equal to the electron concentration. With this normalization condition the mobility in this 1D trap model becomes

$$\tilde{\mu}=\mu F(c,d), \tag{10}$$

where μ is the mobility without traps, d is the electron concentration per site, c is the trap density, $\Delta=E_b-E_a$ is the depth of the trap, and

$$F(c,d)=\left(1+\tfrac{1}{2}\{[(c-d)e^{\beta\Delta}-1] + \sqrt{[1-(c-d)e^{\beta\Delta}]^2+4ce^{\beta\Delta}}\}\right)^{-1}. \tag{11}$$

The field dependence is the same as without the traps but the traps modify the overall magnitude of the mobility. This is an idealized 1D model but it shows the basic physical effect of deep traps and much of the qualitative behavior that we find in the more complete 3D numerical calculations for deep traps is reproduced by this simple 1D model.

IV. 3D NUMERICAL RESULTS

A. Energy distributions and correlations

It is not *a priori* obvious to what extent the 1D results are valid for dense 3D films. In 3D systems a carrier can choose optimal paths to avoid high energy barriers. We study the mobility in a 3D lattice by solving the static Master equation for this system

$$0=\sum_j\left[\omega_{ij}P_j(1-P_i)-\omega_{ji}P_i(1-P_j)\right]. \tag{12}$$

After finding the solution P_i to Eq. (12), we calculate the average carrier velocity from

$$\mathbf{v}=\sum_{ij}\omega_{ji}P_i(1-P_j)\mathbf{R}_{ji}, \tag{13}$$

where $\mathbf{R}_{ji}=\mathbf{r}_j-\mathbf{r}_i$, and obtain the mobility via $\mathbf{v}=\mu\mathbf{E}$. Compared with Monte Carlo simulations[6] the Master equation approach has several advantages: First, it guarantees a stationary solution; second, it is convenient for considering density-dependent effects; third, it is numerically more efficient. In Appendix A, we compare these two numerical approaches in greater detail.

In our numerical calculations, first we generate randomly distributed but spatially correlated molecular geometry fluctuations and, accordingly, polaron energies on each site. Then we solve the Master equation using a symmetric hopping rate in the presence of an applied electric field $\mathbf{E}$,

$$\omega_{ji}=\omega_0 e^{-2\Gamma R_{ij}/a}e^{(\beta/2)[\varepsilon(\mathbf{r}_i)-\varepsilon(\mathbf{r}_j)-e\mathbf{E}\cdot\mathbf{R}_{ji}]}. \tag{14}$$

In Sec. IV, we compare results using this symmetric form for the hopping rate with the small polaron form and the asymmetric Miller-Abrahams form.

We consider nearest and the next nearest neighbor hopping. The system size is $64\times32\times32$, the lattice constant is $a=10$ Å, $2\Gamma=10$, and the applied field is along the x axis. There is no correlation between $\Phi(\mathbf{q})$ for different $\mathbf{q}$. We work in momentum space and generate Gaussian distributions of $\Phi(\mathbf{q})$ with $\mathbf{q}$-dependent width $\Omega[\beta(K\mathbf{q}^2+s)]^{-1}$. Then we Fourier transform to find $\phi(\mathbf{r})$, which have the spatial correlation in Eq. (4).

We use an intermolecular force constant of $K=0.0034$ eV/Å and a coupling coefficient of $\nu=0.3$ eV per radian. These values match the measured room temperature mobility for MEH-PPV and are consistent with the AM1 calculations described above. Here s is set to zero and the temperature is $T=300$ K. The energy distribution is calculated by

$$\rho(\zeta)=\Omega^{-1}\int d^3r\langle\delta(\zeta-\varepsilon(\mathbf{r}))\rangle. \tag{15}$$

We show that the energy distribution $\rho(\zeta)$ is Gaussian by introducing $\theta=\zeta/\nu$,

$$\rho(\zeta)=(\nu\Omega)^{-1}\int d^3r\langle\delta(\theta-\phi(\mathbf{r}))\rangle. \tag{16}$$

Using the Fourier transform, we have

$$\rho(\zeta)=(\nu\Omega)^{-1}\int d^3r\left\langle\delta\left(\theta-\Omega^{-1}\sum_{\mathbf{q}}\Phi(\mathbf{q})e^{-i\mathbf{q}\cdot\mathbf{r}}\right)\right\rangle$$
$$=\frac{1}{2\pi\nu\Omega}\int d^3r\int dx e^{ix\theta}\left\langle e^{-ix\Omega^{-1}\sum_{\mathbf{q}}\Phi(\mathbf{q})e^{-i\mathbf{q}\cdot\mathbf{r}}}\right\rangle. \tag{17}$$

Since there is no correlation between $\Phi(\mathbf{q})$ for different $\mathbf{q}$, the average can be calculated for each $\mathbf{q}$ separately,

$$\langle e^{-ix\Omega^{-1}\Phi(\mathbf{q})e^{-i\mathbf{q}\cdot\mathbf{r}}}\rangle=e^{-(x^2/2\Omega^2)\langle|\Phi(\mathbf{q})|^2\rangle}. \tag{18}$$

Thus

$$\rho(\zeta)=\frac{1}{2\pi\nu}\int dx e^{ix\theta}\prod_{\mathbf{q}}e^{-(x^2/2\Omega^2)\langle|\Phi(\mathbf{q})|^2\rangle}$$
$$=\frac{\sqrt{\pi}}{2\pi\nu b}\exp\left(-\frac{\zeta^2}{4b^2\nu^2}\right), \tag{19}$$

where $b^2=(2\Omega)^{-2}\Sigma_{\mathbf{q}}\langle|\Phi(\mathbf{q})|^2\rangle$. The polaron has a Gaussian energy distribution with a width proportional to ν.

B. Dilute carrier density limit

Previously, we considered the field-dependent mobility in the dilute carrier density limit by linearizing the Master equation.[11] We found that the calculated logarithm of mobility as a function of $E^{1/2}$ was reasonably close to the linear, showing that the model gives approximately the Poole–Frenkel form. For a more dispersive system (e.g., $\nu=0.3$ eV), the mobility was low with a strong field dependence (i.e., larger coefficient multiplying $E^{1/2}$ in the exponential), whereas for a more ordered system (e.g., $\nu=0.1$ eV), the mobility was higher with a weaker field dependence.

Figure 1 describes the effects of temperature on mobility. We calculate the mobility for $T=200$, 300, and 400 K with other parameters fixed. We find that in the low-field regime, with increasing temperature, the mobility is enhanced, whereas in the high-field regime, the mobility decreases with increasing temperature. In the low-field regime, thermal excitations are more important for carriers to overcome the energy barriers than the applied field, and the mobility is larger for higher temperatures. In the high-field regime, however, field-assisted hopping is dominant over the thermal-assisted hopping. For higher temperatures, thermal fluctuations in molecular geometry are stronger and the system becomes more disordered. Therefore in the high-field regime, the mobility is reduced with increasing temperature. In the inset of Fig. 1, we plot the polaron energy distribution at the different temperatures.

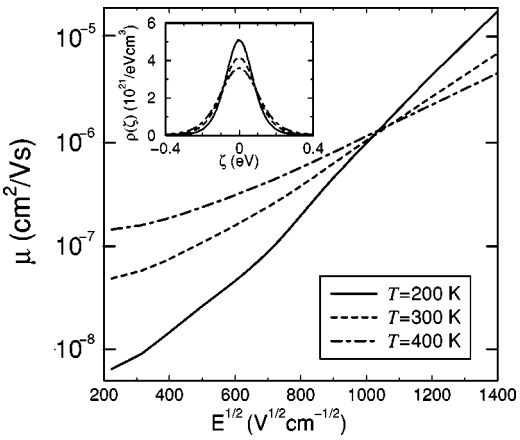

FIG. 1. Logarithm of mobility μ against $E^{1/2}$ with different temperatures for $\nu=0.3$ eV, $K=0.0034$ eV/Å. Solid, dashed, and dot-dashed lines correspond to $T=200$, 300, and 400 K, respectively. The inset is the distribution of carrier energies at these temperatures.

C. Finite carrier density

Sites with the deeper energy potentials are bottlenecks for transport, since it is difficult for carriers to escape once they are caught there. The mobility depends on the carrier density, since when some carriers fill the deeper potentials, the other carriers become more mobile. The density dependence of mobility can be studied by solving the nonlinear Master equation. We have developed an iteration approach to accurately solve these nonlinear equations. From the Master equation (12), we express P_i as

$$P_i=\frac{\sum_j\omega_{ij}P_j}{\sum_k\omega_{ki}}\Bigg/\left\{1-\frac{\sum_j(\omega_{ji}-\omega_{ij})P_j}{\sum_k\omega_{ki}}\right\}. \tag{20}$$

In Eq. (20), we scale all hopping rates by $\Sigma_k\omega_{ki}$ to avoid very large or small numbers. Based on the above equation, we update P_i using *implicit* iterations until the accuracy criterion has been satisfied. Specifically, if we have obtained P_i^{n-1} $(1\leqslant i\leqslant N)$ as the solution after step $n-1$, then to calculate P_i at the next step (step n), on the right hand side of Eq. (20), we will use P_j^n for $j<i$ and P_j^{n-1} for $j>i$. We find that if we use *explicit* iteration, i.e., P_j^{n-1} for all j, the iteration scheme does not converge.

Previously we have illustrated the carrier density effects on the mobility for the case of no trap states.[11] We note that the mobility was enhanced by almost one order of magnitude with increase of the carrier density to $n=6.9\times10^{18}$ cm^{-3} at $E\sim4\times10^4$ V/cm. In the low-field regime, where the field-assisted hopping for carriers is less efficient than in the high-field regime, the carrier density effect on mobility was more pronounced.

In Fig. 2, we illustrate the carrier occupation as a function of the carrier energy with different applied fields. The occupation function is calculated by

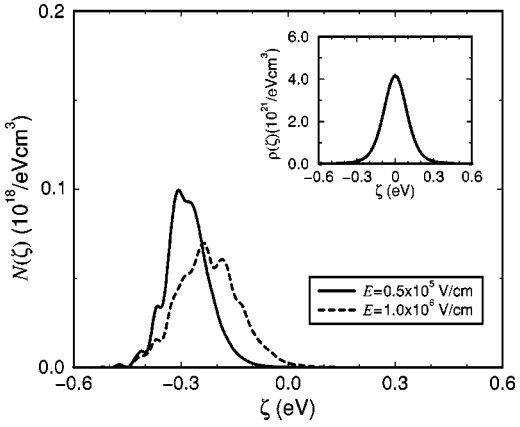

FIG. 2. Carrier occupation as a function of the energy with different applied fields for carrier density $n=6.9\times10^{18}$ cm^{-3}, $\nu=0.3$ eV, $K=0.0034$ eV/Å, and $T=300$ K. Solid and dashed lines correspond to field $E=0.05$ and 1.0×10^{6} V/cm, respectively. The inset is the distribution of carrier energies.

$$N(\zeta)=\Omega^{-1}\sum_i \langle P_i \delta(\zeta-\varepsilon(\mathbf{r}_i))\rangle. \tag{21}$$

We find that the occupation shifts toward higher energy and becomes broader with increasing field. Thus it is more likely that the low-energy sites (traps) are filled by carriers in the low-field regime, where the mobility strongly depends on the carrier density.

Figure 3 shows the effect of deep traps on the mobility. In the system, there are randomly distributed traps with a concentration 0.2×10^{18} cm^{-3} and the trap level is -0.5 eV. Because of the traps, the mobility is small in the low-field regime for low carrier densities. When the carrier density is sufficiently large to quench the traps, the mobility is enhanced dramatically. The field dependences of the mobilities for different carrier densities are similar, which is consistent with the 1D trap model.

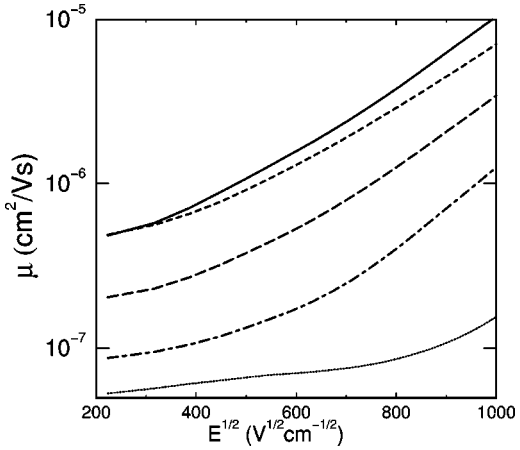

FIG. 3. Logarithm of mobility μ against $E^{1/2}$ with different carrier densities for a system with randomly distributed traps. The trap concentration is 0.2×10^{18} cm^{-3} and the trap level is -0.5 eV. Short-dashed, long-dashed, dot-dashed, and dotted lines correspond to carrier densities $n=0.47$, 0.24, 0.12, 0.03×10^{18} cm^{-3}, respectively. The solid line shows the results of solving the linearized Master equation without traps.

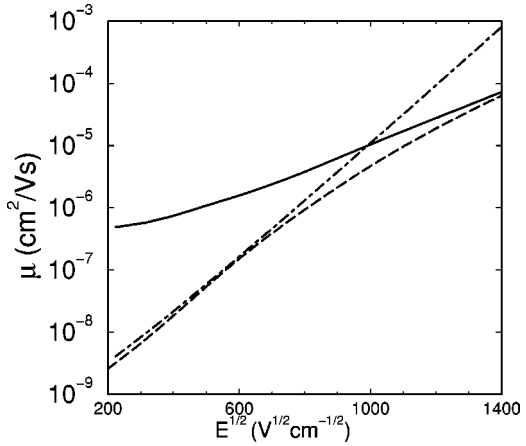

FIG. 4. Logarithm of mobility μ against $E^{1/2}$ for $\nu=0.3$ eV, $K=0.0034$ eV/Å, and $T=300$ K. Solid line is obtained by solving the 3D static Master equation; the dashed line is the numerical 1D result and the dot-dashed line is the analytical 1D result.

D. Comparison between 3D and 1D systems

In Fig. 4, we compare a 3D numerical result, a 1D numerical result, and an analytic 1D result which used Derrida's solution[12] to the 1D Master equation with a continuum approximation to calculate the mobility. For the 1D numerical result we used a solution for a 3D lattice with the same energy distribution as in the 3D numerical calculation but removed all the interchain hopping. We find that the 3D and the 1D numerical results merge in the high-field regime. In the low-field regime, however, the difference is substantial, indicating that the 1D mobility solution cannot be directly extended to 3D systems in the low-field regime. The 1D analytic result is similar to the 1D numerical result at lower fields but differs at higher fields because the continuum approximation was used in the analytical result.

In 3D systems, a carrier can optimize its path to avoid high energy barriers and achieve a higher mobility. Figure 5 illustrates the current patterns in the low-field and the high-field regions. In the figure, we project the 3D lattice onto the x-y plane by summing over the currents in different planes. The width of each bond in the figure is proportional to the current across the bond. Darker bonds indicate that the current is opposite to the standard directions (from left to right and from down to up). In the low-field regime, we see that the carriers take complex paths involving many chains. When such irregular paths occur, a 1D model, where the path is always along the field, is not appropriate. In the high-field regime, where the field is strong enough to overcome the energy barriers, the carrier paths are essentially one-dimensional. Therefore the 3D and 1D numerical results merge in the high-field regime.

E. Correlation length effects

In the above calculations, the intramolecular restoring force s was set to zero. Finite values for s results in a short-

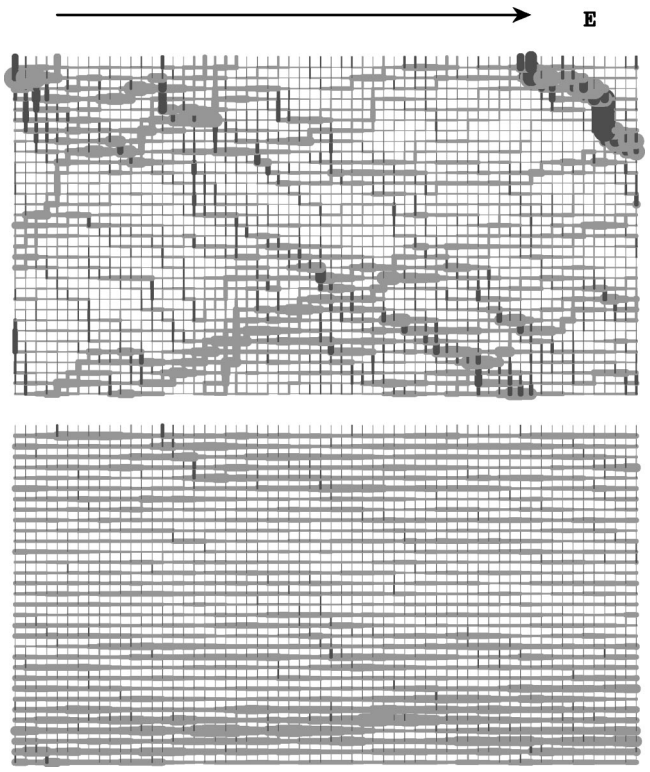

FIG. 5. Current patterns (carrier paths) for different applied field. The width of the bond is proportional to the current across this bond. Upper and lower panels are for $E=0.5\times10^5$ and 2×10^6 V/cm, respectively.

range energy correlation $\sim e^{-\alpha R}$. In Fig. 6, we plot the mobility as a function of the applied field for different values of α but with identical energy distributions as shown in the inset of Fig. 2. Thus these different curves correspond to the same disorder strength but different energy correlations. $\alpha=0$ means that the polaron energy has a long-range correlation. $\alpha=1.0$ Å^{-1} indicates that the polaron energy is virtually uncorrelated, which is very close to the GDM model. We find that with increasing α, the mobility decreases rapidly and the mobility deviates from the Poole-Frenkel behavior in the low-field region. These results demonstrate that the energy correlation can enhance the mobility efficiently and make the field dependence of the mobility closer to the Poole-Frenkel behavior.

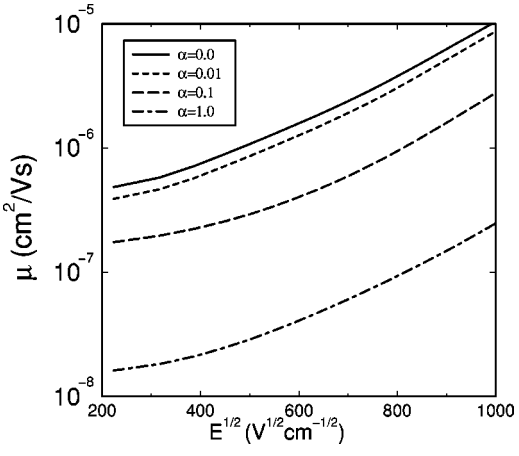

FIG. 6. Logarithm of mobility μ against $E^{1/2}$ for $\nu=0.3$ eV and $T=300$ K. K is adjusted for different intramolecular restoring constants s in such a way to keep the same energy distribution as in the inset of Fig. 2. Solid, short-dashed, long-dashed, and dot-dashed lines correspond to $\alpha=0$, 0.01, 0.1, and 1.0 Å^{-1}, respectively.

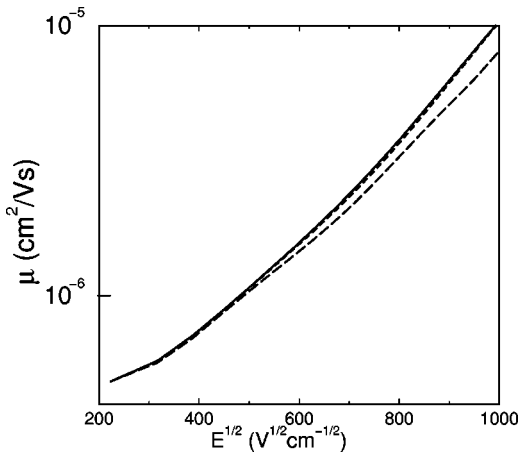

FIG. 7. Comparison of calculated mobility using the symmetric hopping rate and the small-polaron rates. The solid line is for the symmetric hopping rates. The short-dashed and long-dashed lines are for the small polaron hopping rates with $\Omega=0.1$ and 0.02 eV, respectively. Other parameters are fixed, $\nu=0.3$ eV, $K=0.0034$ eV/Å, and $T=300$ K.

F. Small-polaron and Miller-Abrahams hopping rates

In the foregoing calculations, the rate with which a carrier hops from one site to another was chosen to be the widely used symmetric form of Eq. (14). This form corresponds to the small-polaron hopping rate for systems with a strong charge-lattice coupling.

According to the small-polaron theory developed by Holstein and Emin,[18,19] the hopping rate can be written as

$$\omega_{ji}\propto\sqrt{\frac{\beta}{4\pi\Omega}}e^{-2\Gamma(R_{ij}/a)}e^{-(\beta/4\Omega)(\Delta\varepsilon_{ji}+\Omega)^2}, \qquad (22)$$

where $\Delta\varepsilon_{ji}=\varepsilon_j-\varepsilon_i-e\mathbf{E}\cdot\mathbf{R}_{ji}$ is energy difference between sites j and i in the presence of an applied electric field $\mathbf{E}$ and Ω is the small-polaron relaxation energy. When $\Delta\varepsilon_{ji}\ll\Omega$, the small-polaron hopping rate reduces to the symmetric form of Eq. (14) within site-energy-independent terms that can be included in ω_0.

When Ω is comparable to or smaller than $\Delta\varepsilon_{ji}$, it is not clear that the hopping rate in Eq. (14) is a good approximation to the small-polaron form. To see how much difference these two forms of hopping rates make in the mobility calculations, we carry out calculations using the small-polaron hopping rates with different values for Ω. We adjust an overall multiplicative factor to give the same low-field mobility results and compare the field dependences for the different hopping rates. As shown in Fig. 7, these different hopping rates lead to very similar field dependence over the

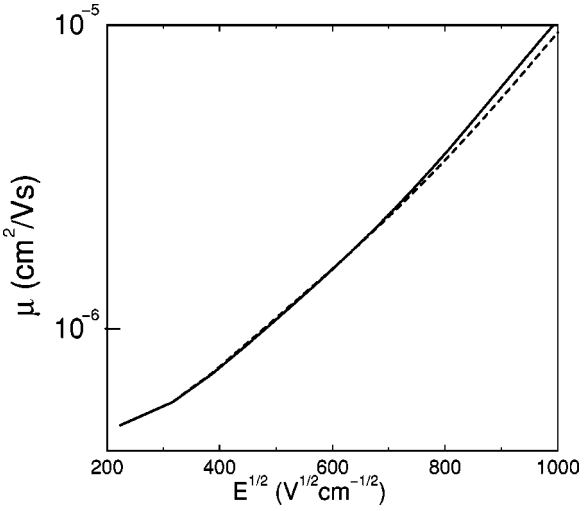

FIG. 8. Comparison of the calculated mobility using symmetric and asymmetric hopping rates. The solid line is obtained by using the symmetric hopping rate with $\nu=0.3$ eV, $K=0.0034$ eV/Å, and $T=300$ K. The dashed line is obtained by using the asymmetric Miller-Abrahams hopping rate.

range of fields considered even when $\Omega=0.02$ eV, smaller than the width of energy distribution (~ 0.1–0.2 eV at $\nu=0.3$ eV). We conclude that the symmetric form of Eq. (14) is reasonable to study the field-dependent mobility in dense polymer films for the range of fields commonly used in polymer based electronic devices.

In the literature of transport in disordered systems, an asymmetric rate with the Miller-Abrahams form has also been extensively used,

$$\omega_{ji}=\omega_0 e^{-2\Gamma(R_{ij}/a)}\begin{cases} e^{-\beta\Delta\varepsilon_{ji}}, & \text{if } \Delta\varepsilon_{ji}>0 \\ 1, & \text{if } \Delta\varepsilon_{ji}<0. \end{cases} \tag{23}$$

Both the symmetric form Eq. (14) and the asymmetric Miller-Abrahams form Eq. (23) satisfy the detailed balance,

$$\frac{\omega_{ji}}{\omega_{ij}}=\exp(-\beta\Delta\varepsilon_{ji}). \tag{24}$$

We compare the mobility calculated using the asymmetric Miller-Abrahams hopping rates and symmetric hoppings. Figure 8 shows that the calculated mobility is not sensitive to the choice of hopping rates over the range of fields considered.

V. CONCLUDING REMARKS

In summary, we proposed a general model to describe transport in dense films of conjugated polymers. In this model thermal fluctuations in the molecular geometry modify the energy levels of localized electronic excitations in the material. Based on quantum chemistry calculations we argue that the primary restoring force for these fluctuations in molecular geometry is steric in origin. Because the restoring force is intermolecular, there is a spatial correlation in the molecular distortions. This leads to spatially correlated fluctuations in the on-site energy of the electronic excitations. The phenylene ring torsion, in PPV-like conjugated polymers, is an example of this kind of spatially correlated thermal fluctuation.

We developed a numerical approach which enables us to study the electrical transport in three-dimensional systems. We investigated the density dependence of the mobility and find that when the carrier density is large, the mobility can be significantly enhanced. The mobility increases strongly with increasing carrier density at low fields, but carrier density dependence of the mobility is weaker at high fields. These results are consistent with both light-emitting diodes and field-effect transistor measurements. We also studied the mobility in a system with randomly distributed traps. We found that the trap affects primarily the overall magnitude of the mobility and has a weaker effect on the field dependence of the mobility. When the carrier density is sufficiently large to fill up all traps, the mobility is enhanced.

We found that the carrier hopping in the low-field regime is mainly due to the thermal excitations, while in the high-field regime, the field-assisted hopping becomes dominant. These different hopping mechanisms result in different temperature dependences in different field regions: In the low-field regime, the mobility increases as temperature increases, whereas in the high-field regime, the mobility decreases as temperature increases.

We compared our 3D numerical results with 1D numerical results and 1D analytical results. We studied typical carrier paths at different electric fields. We found that, in the low-field regime, the carrier paths are irregular and distributed in the whole 3D system, whereas in the high-field regime, the path is essentially 1D along the field. We found that the mobilities from our 3D numerical result and the 1D numerical one are close to each other at high fields but dramatically different in the low-field region, indicating that 1D models cannot be directly extended to 3D systems at low fields. Finally, we studied the effect of asymmetric hopping rate and small-polaron rate on the mobility. We found that these two variables do not significantly affect the mobility compared to the case of symmetric hopping rate.

Our model presents a comprehensive picture and a general framework for understanding the Poole-Frenkel behavior observed in many conjugated polymers. Our numerical calculations provide an understanding of carrier density, temperature, and trap effects on the field-dependent mobility in these materials.

ACKNOWLEDGMENTS

We are grateful to I. H. Campbell, E. M. Conwell, D. H. Dunlap, and S. V. Novikov for helpful discussions. This work was supported by the Molecularly Engineered Electronic Materials program at Los Alamos National Laboratory and the U. S. Department of Energy.

APPENDIX A: COMPARISON BETWEEN MONTE CARLO AND MASTER EQUATION APPROACHES

In previous numerical studies of field-dependent mobility in polymers, Monte Carlo simulations have been widely used

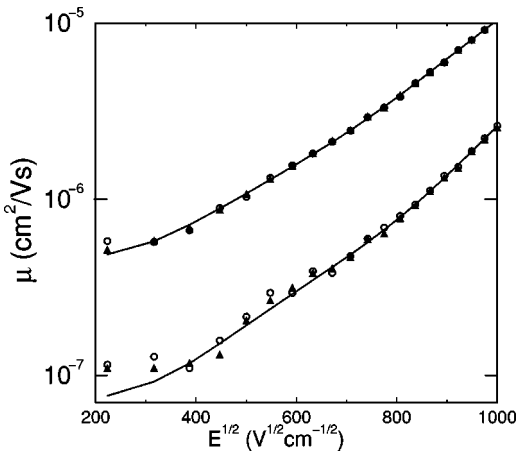

FIG. 9. Comparison between the Monte Carlo and the Master equation approaches. The two solid lines are obtained by solving the static Master equations with $\nu=0.3$ (upper one) and 0.35 eV (lower one). The open circles and filled triangles are Monte Carlo results. The simulation time is t_0 for open circles and $2t_0$ for filled triangles.

because they are both conceptually simple and easily programmed.[5–7,10] In this approach, at $t=0$ some particles are added in a lattice, these particles then randomly hop to adjacent sites according to a particular distribution. The mobility is determined by calculating the average velocity of particles after a simulation time t_0. Thus t_0 must be long enough so that the average velocity will not change if a longer simulation time was used.

Since the mobility is a property of the steady state, one can directly solve the stationary Master equation to study the mobility. Compared with the Monte Carlo simulations, the Master equation approach has the advantage that stationary solutions are guaranteed. Since the Monte Carlo simulation time required for convergent results increases exponentially as the disorder becomes stronger in the systems,[6] it is difficult to obtain stationary solutions from the Monte Carlo simulations for strongly disordered systems. As an example, we carry out Monte Carlo simulations to calculate the mobility using our model. We choose t_0 large enough that for weak disorder strengths ($\nu=0.1$ and 0.2 eV), the Monte Carlo simulations produce exactly the same results as the Master equation approach. For stronger disorder strengths ($\nu=0.3$ and 0.35 eV), as shown in Fig. 9, the results from Monte Carlo simulations deviate somewhat from those from the Master equation approach. If we double the simulation time, the Monte Carlo results approach the Master equation results but deviation still exists. This comparison indicates that the Monte Carlo simulations can become inefficient in polymers with strong disorder.

APPENDIX B: DISTRIBUTION FUNCTION FOR THE MOLECULAR GEOMETRY FLUCTUATIONS: INTERACTION WITH THE CARRIER

The distribution function we use to describe fluctuations in the classical molecular geometry field is based on the free energy expression in Eq. (3). It is rigorously valid only in the weak coupling limit (i.e., small ν) because the interactions with the carrier, described by the term linear in the classical field variable, are not included in the expression for the free energy. This term may not be negligible for realistic values of the model parameters for polymers. Here we show that the effects of this coupling can be included by taking the expectation value of the Hamiltonian with the carrier at a specific molecular site and completing the square to eliminate the linear term in the classical field variable. This treatment again gives a Gaussian distribution function with a modified classical field variable. The results are essentially the same as the original treatment in that the long-range spatial correlations are maintained and with the same functional form.

Consider that part of the Hamiltonian which involves only the molecular geometry field ϕ and its coupling with the charge of a carrier at site i:

$$E=\frac{K}{2}\int d^3r(\nabla\phi)^2+\nu\int d^3r\,\phi(\mathbf{r})|\psi_i(\mathbf{r})|^2+\frac{s}{2}\int d^3r\,\phi^2(\mathbf{r}),$$

which can be rewritten in the Fourier transformed form as

$$E=\Omega^{-1}\sum_{\mathbf{q}}\left\{|\Phi(\mathbf{q})|^2\left[\frac{K\mathbf{q}^2+s}{2}\right]+\nu\Phi(\mathbf{q})R_i(\mathbf{q})\right\},$$

with

$$R_i(\mathbf{q})=\int d^3r e^{-i\mathbf{q}\cdot\mathbf{r}}|\psi_i(\mathbf{r})|^2.$$

We can further simplify this by completing the square

$$E=\Omega^{-1}\sum_{\mathbf{q}}\left[|\bar{\Phi}(\mathbf{q})|^2\left(\frac{K\mathbf{q}^2+s}{2}\right)-\frac{\nu^2|R_i(\mathbf{q})|^2}{2(K\mathbf{q}^2+s)}\right],$$

where

$$\bar{\Phi}(\mathbf{q})=\Phi(\mathbf{q})+\frac{\nu R_i^*(\mathbf{q})}{K\mathbf{q}^2+s}.$$

Picking $\Phi(\mathbf{q})$ according to the distribution function defined by this free energy expression, with the relation between $\bar{\Phi}(\mathbf{q})$ and $\Phi(\mathbf{q})$ given above, gives the same site energy distribution as the procedure we used (to within an overall constant) as long as the wave functions on the sites are the same.

[1] J. H. Burroughes, D. D. C. Bradley, A. R. Brown, R. N. Marks, K. MacKay, R. H. Friend, P. L. Burns, and A. B. Holmes, Nature (London) **347**, 539 (1990).

[2] J. R. Sheats, H. Antoniadis, M. Hueschen, W. Leonard, J. Miller, R. Moon, D. Roitman, and A. Stocking, Science **273**, 884 (1996).

[3] I. H. Campbell, D. L. Smith, C. J. Neef, and J. P. Ferraris, Appl. Phys. Lett. **74**, 2809 (1999).

[4] P. W. Blom, M. J. M. Dejong, and M. G. VanMunster, Phys. Rev. B **55**, R656 (1997).
[5] M. Abkowitz, H. Bässler, and M. Stolka, Philos. Mag. B **63**, 201 (1991).
[6] H. Bässler, Phys. Status Solidi B **175**, 15 (1993).
[7] Yu. N. Gartstein and E. M. Conwell, Chem. Phys. Lett. **245**, 351 (1995).
[8] D. M. Pai, J. Chem. Phys. **52**, 2285 (1970).
[9] W. D. Gill, J. Appl. Phys. **43**, 5033 (1972).
[10] D. H. Dunlap, P. E. Parris, and V. M. Kenkre, Phys. Rev. Lett. **77**, 542 (1996); S. V. Novikov, D. H. Dunlap, V. M. Kenkre, P. E. Parris, and A. V. Vannikov, *ibid.* **81**, 472 (1998).
[11] Z. G. Yu, D. L. Smith, A. Saxena, R. L. Martin, and A. R. Bishop, Phys. Rev. Lett. **84**, 721 (2000).
[12] B. Derrida, J. Stat. Phys. **31**, 433 (1983).
[13] M. Redecker, D. D. C. Bradley, M. Inbasekaran, and E. P. Woo, Appl. Phys. Lett. **73**, 1565 (1998).
[14] D. Chen, M. J. Winokur, M. A. Masse, and F. E. Karasz, Phys. Rev. B **41**, 6759 (1990).
[15] K. Pichler, D. A. Halliday, D. D. C. Bradley, P. L. Burn, R. H. Friend, and A. B. Holmes, J. Phys.: Condens. Matter **5**, 7155 (1993).
[16] H. J. S. Dewar, E. G. Zoebisch, and E. F. Healy, J. Am. Chem. Soc. **107**, 3902 (1985).
[17] P. E. Parris, M. Kuś, D. H. Dunlap, and V. M. Kenkre, Phys. Rev. E **56**, 5295 (1997).
[18] T. Holstein, Ann. Phys. (N.Y.) **8**, 325 (1959); **8**, 343 (1959).
[19] D. Emin, Adv. Phys. **24**, 305 (1975).